Real-Time Drag Optimization of Aspect Ratio 13.5 Common Research Model with Distributed Flap System

Nhan Nguyen*
NASA Ames Research Center, Moffett Field, CA 94
Juntao Xiong†
KBR Wyle, Inc., Moffett Field, CA 94035

This paper presents a real-time drag optimization study of the aspect ratio 13.5 Common Research Model (CRM) with a distributed mini-plain flap system. A surrogate aerodynamic model of the aspect ratio 13.5 CRM is developed based on an aerodynamic database computed by a transonic panel method to capture the aerodynamic coefficients as functions of the angle of attack, flap deflections, and Mach number. A recursive least-squares parameter estimation algorithm is designed to estimate the aerodynamic parameters of the surrogate model. The estimated surrogate model is then used in an on-line drag optimization strategy based on an adjoint method. The results of the real-time drag optimization indicate a drag reduction of 2.46% for Mach 0.80, 3.37% for Mach 0.85, and 1.95% for Mach 0.88. The results show the convergence of all parameter estimates.

I. Introduction

The aircraft industry has been responding to the need for more energy-efficient aircraft by redesigning airframes to be aerodynamically and structurally more efficient, employing lightweight advanced composite materials for aircraft structures, and incorporating more energy-efficient aircraft engines. Reducing airframe operational empty weight using advanced composite materials is one of the major considerations for improving energy efficiency. The Boeing 787 transport is an example of a modern airframe design that employs lightweight structures. Modern lightweight materials can provide less structural rigidity while maintaining sufficient load carrying capacity. As structural flexibility increases, aeroelastic interactions with aerodynamic forces can adversely affect the aircraft performance significantly. The increase in the wing aspect ratio in the modern transport aircraft also exacerbates the aeroelastic problem as the wing twist under load can be substantial. This causes the optimal lift distribution for low-drag performance to deviate substantially throughout the flight envelope. Cruise drag optimization control becomes necessary to compensate for the aeroelastic penalty.

In the current practice, cruise drag optimization in modern transport design is implemented as a table-lookup method for scheduling flap settings as a function of the aircraft gross weight, airspeed, and altitude. The table-lookup method generally depends on a validated analytical model of the reference geometry of a particular aircraft design. The analytical model must be validated with wind tunnel and flight test data to ensure the accuracy of the performance prediction. Aircraft production variances, however, can result in varying performance characteristics among aircraft. Different operating conditions such as gross weight, airspeed, and altitude could also contribute to the variability of the aircraft performance. All of these possible variations can result in a wide range of performance characteristics and uncertainty in the table-lookup method.

Real-time drag optimization strategy could hold promise and could provide more flexibility than the table-lookup method. It is perhaps the ultimate goal of the adaptive wing vision to make aircraft 'smarter' and truly mission-adaptive. However, many technical hurdles must be overcome in order to realize this vision. In a larger picture, such a strategy must be able to predict the aerodynamic performance very accurately by estimation using only data from sensors and flap inputs. The sensors themselves must be able to reliably and accurately measure the aerodynamic performance parameters. The performance estimation has to be coupled to the flight control system which sends

*Senior Research Scientist and Technical Group Lead of Advanced Control and Engineering Systems Group, Intelligent Systems Division, nhan.t.nguyen@nasa.gov
†Aerospace Engineer, Intelligent System Division, juntao.xiong@nasa.gov

commands to the flap actuators. The real-time drag optimization must be able to compute in real-time the optimal flap configuration and aircraft states. Then, the outputs from the real-time drag optimization are to be translated into commands to be processed by the aircraft flight control system and or flight management system. This strategy has been examined in a recent study which proposes a real-time model identification technique based on the recursive least-squares method to construct an on-line surrogate aerodynamic model of a flexible wing aircraft.[1] A wind tunnel test has been conducted in 2017 and 2018 to validate the real-time drag optimization strategy. This test successfully demonstrates the real-time drag optimization which was able to achieve up to 9.4% drag reduction for off-design cruise conditions.[2,3]

This paper further explores this real-time drag optimization strategy for an aspect ratio 13.5 Common Research Model (CRM) developed by Boeing under a NASA contract with the NASA Advanced Air Transport Technology project. The aspect ratio 13.5 CRM is developed from the original aspect ratio 8.3 CRM.[4] The aspect ratio 13.5 CRM configuration employs a distributed mini-plain flap system which comprises 11 small trailing edge flaps positioned along the wing span. These mini-plain flaps can be used for a drag optimization strategy. Figure 1 illustrates the aspect ratio 13.5 CRM configuration.

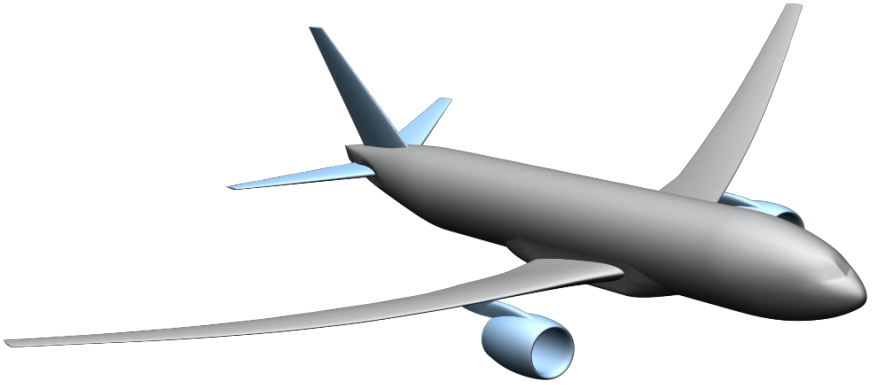

Figure 1. Aspect Ratio 13.5 Common Research Model (Credit: The Boeing Company)

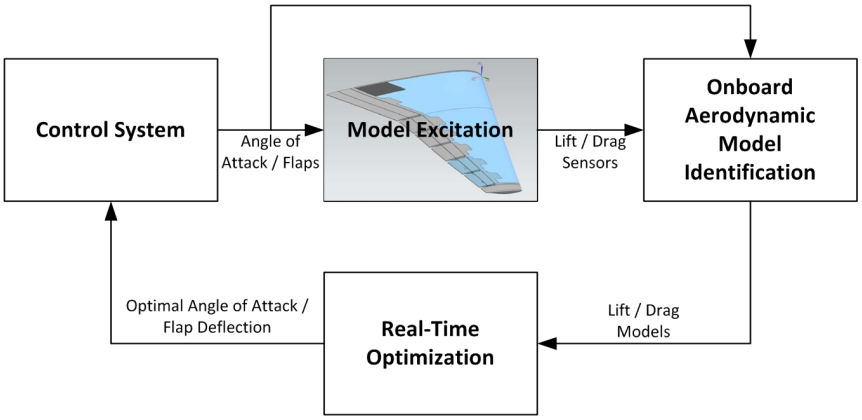

Figure 2. Real-Time Drag Optimization Framework

Figure 2 illustrates a real-time drag optimization framework which comprises a control system, an onboard aerodynamic model identification, a model excitation, and a real-time drag optimization. The control system sends command signals to the wing to change the angle of attack and flap positions. The onboard aerodynamic model identification performs a real-time parameter estimation via a recursive least-squares (RLS) algorithm to estimate the sensitivities of the lift, drag, and pitching moment coefficients with respect to the angle of attack and individual flap positions. These aerodynamic sensitivities are then used to construct an onboard surrogate aerodynamic model for use in the real-time drag optimization. The model excitation provides an input set of commands of the angle of attack and flap positions.

The real-time drag optimization performs the optimization to minimize the trim drag for a target off-design trim lift coefficient. The real-time drag optimization is based on an adjoint method.

II. Aerodynamic Database and Onboard Model

The aerodynamic model is provided by Boeing. The data comprises the lift, drag, and pitching moment coefficients as functions of the angle of attack, the flap deflections, and the elevator deflection for Mach 0.80, 0.85, and 0.88. The database is computed by Boeing TRANAIR code. The baseline aerodynamic data are for the wing-body configuration alone. The aerodynamic coefficients for the mini-plain flaps and the elevator are presented as increments to the aerodynamic coefficients for the wing-body configuration.

Figures 3, 4, 5, 6 respectively show the lift coefficient C_L, the drag coefficient C_D, the pitching moment coefficient C_m, and the lift-to-drag ratio L/D for the clean-wing configuration without flap deployment. It is noticed that the lift and pitching moment coefficients are quite nonlinear with respect to the angle of attack in the normal cruise angle of attack between 1° and 3°.

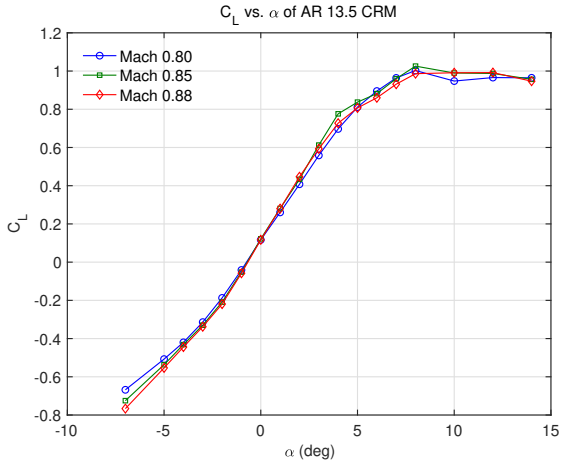

Figure 3. Lift Coefficient C_L vs. Angle of Attack α of AR 13.5 CRM

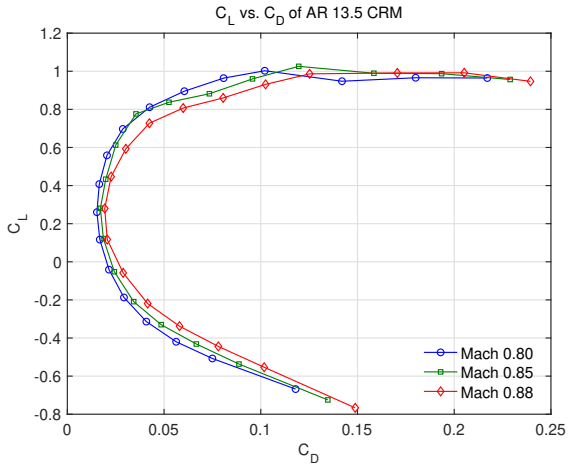

Figure 4. Lift Coefficient C_L vs. Drag Coefficient C_D of AR 13.5 CRM

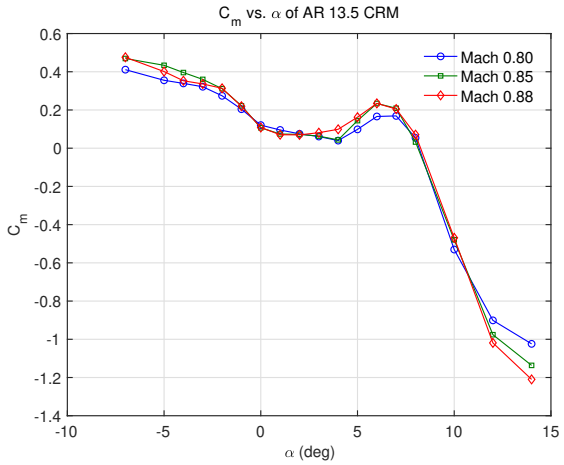

Figure 5. Pitching Moment Coefficient C_m vs. Angle of Attack α of AR 13.5 CRM

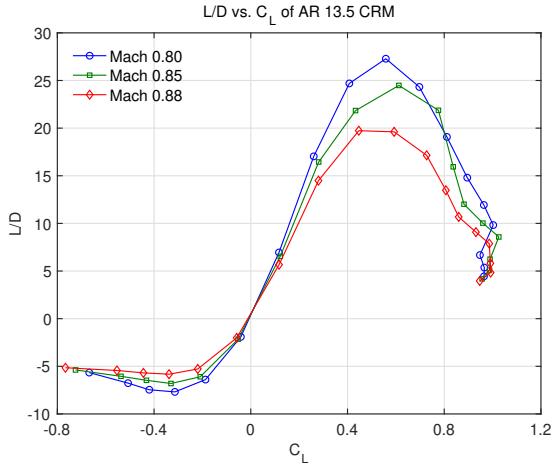

Figure 6. Lift-to-Drag Ratio L/D vs. Lift Coefficient C_L of AR 13.5 CRM

The maximum lift-to-drag ratio L/D ranges from 20 for Mach 0.88 to 27.5 for Mach 0.80 and occurs at a lift coefficient of about 0.56 for Mach 0.80, 0.61 for Mach 0.85, and 0.52 for Mach 0.88. The design lift coefficient is assumed to be 0.5. Therefore, the Mach 0.85 flight condition is further from the design point than the Mach 0.80 and 0.88 flight conditions.

Figures 7, 8, and 9 are the respective plots of the incremental lift, drag, and pitching moment coefficients for Mach 0.80 at the angle of attack of 2° where the aircraft is normally trimmed at. The incremental lift and pitching moment coefficients are generally linear with respect to the flap deflection. The incremental drag coefficient follows a parabolic relationship.

Figures 10, 11, and 12 are the respective plots of the incremental lift, drag, and pitching moment coefficients for Mach 0.85 at the angle of attack of 2° where the aircraft is normally trimmed at. The behaviors of the incremental lift, drag, and pitching moment coefficients follow the same trend as those for Mach 0.80.

Figures 13, 14, and 15 are the respective plots of the incremental lift, drag, and pitching moment coefficients for Mach 0.88 at the angle of attack of 2° where the aircraft is normally trimmed at. The incremental lift coefficient shows a considerable nonlinearity. The incremental pitching moment coefficient also exhibits some degree of nonlinearity.

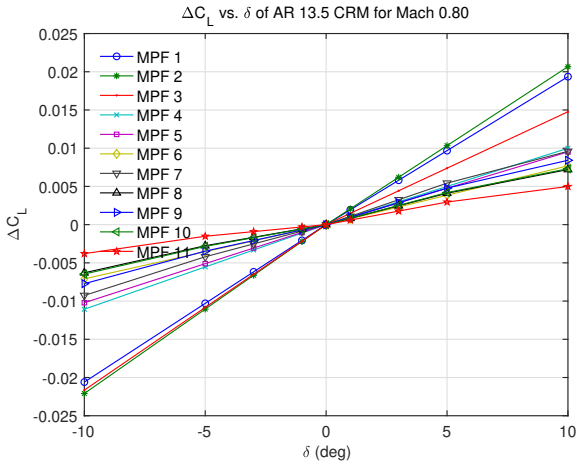

Figure 7. Incremental Lift Coefficient ΔC_L vs. Flap Deflection δ of AR 13.5 CRM at Mach 0.80 and Angle of Attack of 2°

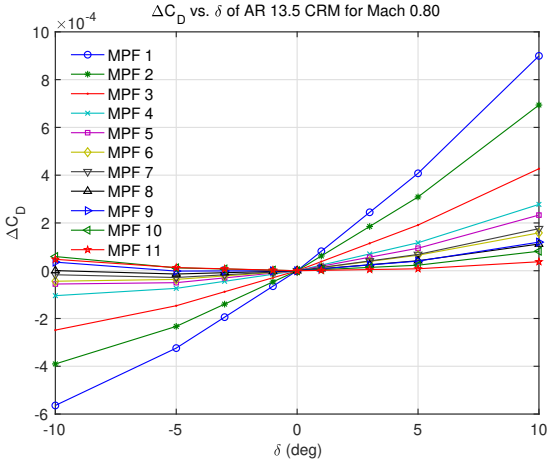

Figure 8. Incremental Drag Coefficient ΔC_D vs. Flap Deflection δ of AR 13.5 CRM at Mach 0.80 and Angle of Attack of 2°

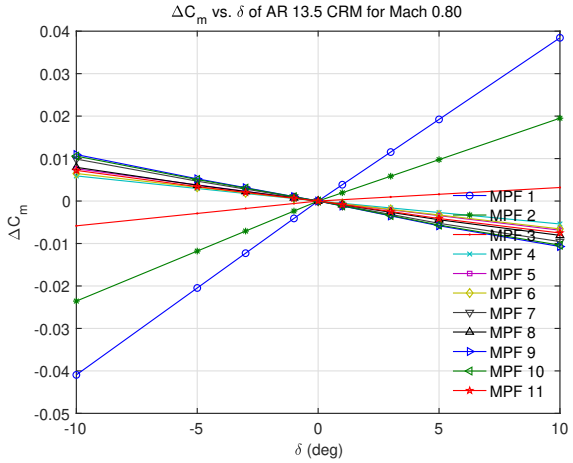

Figure 9. Incremental Pitching Moment Coefficient ΔC_m vs. Flap Deflection δ of AR 13.5 CRM at Mach 0.80 and Angle of Attack of 2°

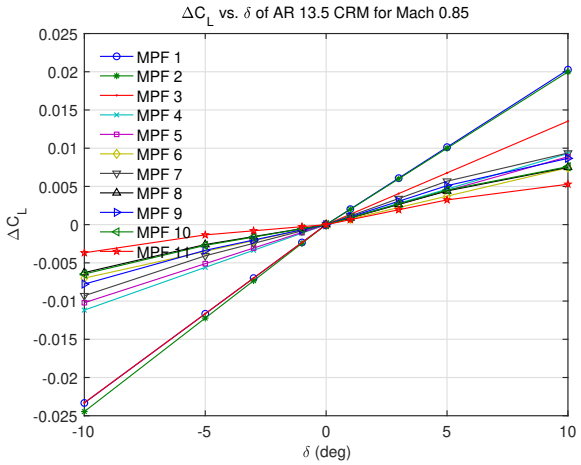

Figure 10. Incremental Lift Coefficient ΔC_L vs. Flap Deflection δ of AR 13.5 CRM at Mach 0.85 and Angle of Attack of 2°

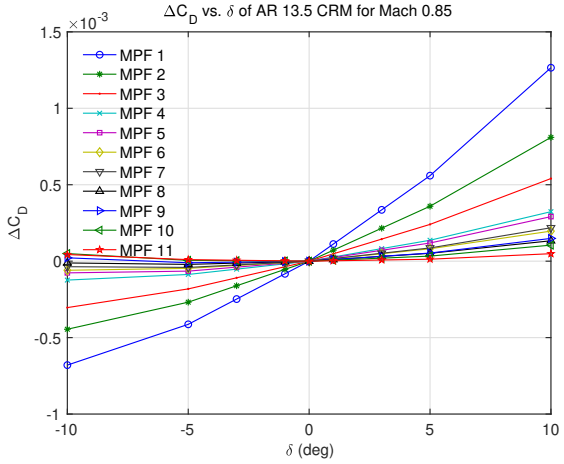

Figure 11. Incremental Drag Coefficient ΔC_D vs. Flap Deflection δ of AR 13.5 CRM at Mach 0.85 and Angle of Attack of 2°

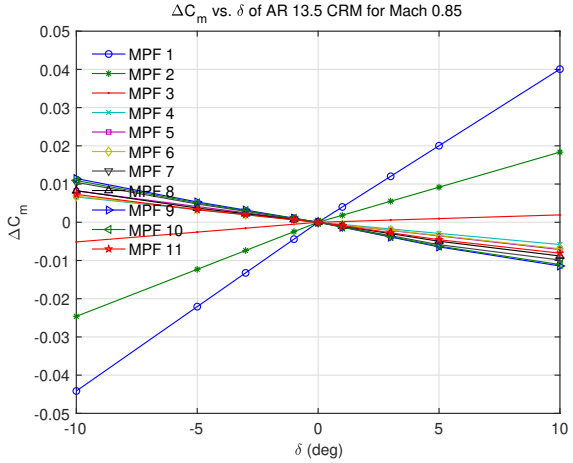

Figure 12. Incremental Pitching Moment Coefficient ΔC_m vs. Flap Deflection δ of AR 13.5 CRM at Mach 0.85 and Angle of Attack of 2°

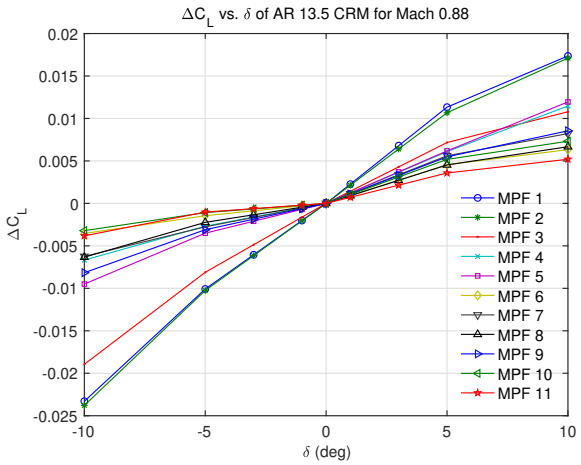

Figure 13. Incremental Lift Coefficient ΔC_L vs. Flap Deflection δ of AR 13.5 CRM at Mach 0.88 and Angle of Attack of 2°

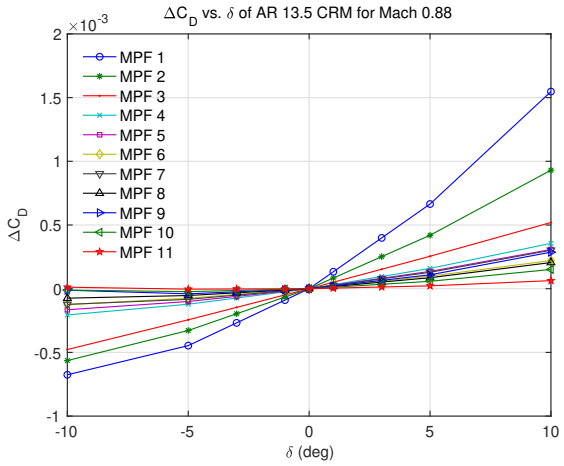

Figure 14. Incremental Drag Coefficient ΔC_D vs. Flap Deflection δ of AR 13.5 CRM at Mach 0.88 and Angle of Attack of 2°

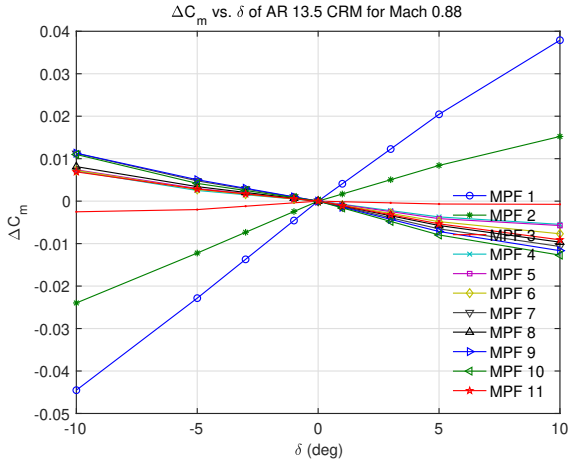

Figure 15. Incremental Pitching Moment Coefficient ΔC_m vs. Flap Deflection δ of AR 13.5 CRM at Mach 0.88 and Angle of Attack of 2°

Based on the aerodynamic database, the following onboard aerodynamic model is used in the real-time drag

optimization:

$$C_L = C_{L_0} + C_{L_\alpha}\alpha + C_{L_\delta}\delta + C_{L_{\delta_e}}\delta_e + C_{L_{\alpha^2}}\alpha^2 + C_{L_{\delta^2}}\delta^2 + C_{L_{\delta_e^2}}\delta_e^2 \tag{1}$$

$$C_D = C_{D_0} + C_{D_\alpha}\alpha + C_{D_\delta}\delta + C_{D_{\delta_e}}\delta_e + C_{D_{\alpha^2}}\alpha^2 + C_{D_{\delta^2}}\delta^2 + C_{D_{\delta_e^2}}\delta_e^2 \tag{2}$$

$$C_m = C_{m_0} + C_{m_\alpha}\alpha + C_{m_\delta}\delta + C_{m_{\delta_e}}\delta_e + C_{m_{\alpha^2}}\alpha^2 + C_{m_{\delta^2}}\delta^2 + C_{m_{\delta_e^2}}\delta_e^2 \tag{3}$$

where $\delta = \begin{bmatrix} \delta_1 & \delta_2 & \cdots & \delta_{11} \end{bmatrix}^\top$ is a vector of the mini-plain flap deflections, $\delta^2 = \begin{bmatrix} \delta_1^2 & \delta_2^2 & \cdots & \delta_{11}^2 \end{bmatrix}^\top$ is a vector of the squares of the mini-plain flap deflections, and δ_e is the elevator deflection.

This model is valid only in the local region around the trim angle of attack of 2°. The nonlinear lift and pitching moment coefficients reflect the nonlinear behaviors exhibited in the aerodynamic database.

III. Recursive Least-Squares Parameter Estimation

The onboard aerodynamic model contains the unknown sensitivities of the lift, drag, and pitching moment coefficients with respect to the angle of attack, the mini-plain flap deflections, and the elevator deflection. These unknown sensitivities are estimated by a recursive least-squares (RLS) parameter estimation algorithm. It is assumed that the lift, drag, and pitching moment coefficients can be synthesized from aircraft sensors. Sensor development is not within the scope of this study. The RLS parameter estimation is performed in a two-stage process. The first stage is to apply an excitation signal to the angle of attack to perturb its value from the current trim position while maintaining all the flap deflections at their current values. This enables all the sensitivities with respect to the angle of attack to be estimated by the RLS algorithm. In the second stage, the angle of attack is maintained at the current trim value, but excitation signals are applied to all the flap deflections to perturb their positions one at a time from their current values.

During the first stage, the angle of attack α is perturbed twice by $\pm\Delta\alpha$ where $\Delta\alpha$ is a chosen increment. During this stage, all the mini-plain flaps δ_j and the elevator δ_e are kept constant. A linear regression can be performed by minimizing the error squared

$$\min J = \sum_{i=1}^{3n} \left(\begin{bmatrix} \Delta C_L \\ \Delta C_D \\ \Delta C_m \end{bmatrix}_i - \begin{bmatrix} C_{L_0} \\ C_{D_0} \\ C_{m_0} \end{bmatrix} - \begin{bmatrix} C_{L_\alpha} \\ C_{D_\alpha} \\ C_{m_\alpha} \end{bmatrix} \alpha_i - \begin{bmatrix} C_{L_{\alpha^2}} \\ C_{D_{\alpha^2}} \\ C_{m_{\alpha^2}} \end{bmatrix} \alpha_i^2 \right)^2 \tag{4}$$

where n is the number of iterations and

$$\begin{bmatrix} \Delta C_L \\ \Delta C_D \\ \Delta C_m \end{bmatrix} = \begin{bmatrix} C_L \\ C_D \\ C_m \end{bmatrix} - \begin{bmatrix} C_{L_\delta} & C_{L_{\delta_e}} \\ C_{D_\delta} & C_{D_{\delta_e}} \\ C_{m_\delta} & C_{m_{\delta_e}} \end{bmatrix} \begin{bmatrix} \bar{\delta} \\ \bar{\delta}_e \end{bmatrix} - \begin{bmatrix} \bar{\delta} & \bar{\delta}_e \end{bmatrix} \begin{bmatrix} C_{L_{\delta^2}} & C_{L_{\delta_e^2}} \\ C_{D_{\delta^2}} & C_{D_{\delta_e^2}} \\ C_{m_{\delta^2}} & C_{m_{\delta_e^2}} \end{bmatrix} \begin{bmatrix} \bar{\delta} \\ \bar{\delta}_e \end{bmatrix} \tag{5}$$

Note that ΔC_L is computed using the current estimates of the aerodynamic sensitivities with respect to the flap deflections and the elevator deflection and their current trim positions $\bar{\delta}$ and $\bar{\delta}_e$.

For brevity, we denote $y_i = \begin{bmatrix} \Delta C_L \\ \Delta C_D \\ \Delta C_m \end{bmatrix}_i$, $\Theta_\alpha = \begin{bmatrix} C_{L_{\alpha^2}} & C_{D_{\alpha^2}} & C_{m_{\alpha^2}} \\ C_{L_\alpha} & C_{D_\alpha} & C_{m_\alpha} \\ C_{L_0} & C_{D_0} & C_{m_0} \end{bmatrix}$, $\Phi(\alpha_i) = \begin{bmatrix} \alpha_i^2 \\ \alpha_i \\ 1 \end{bmatrix}$. Then, the cost function can be written as

$$\min J = \sum_{i=1}^{3n} \left[y_i - \Theta_\alpha^\top \Phi(\alpha_i) \right]^2 \tag{6}$$

Taking the partial derivative of the cost function with respect to the parameter matrix Θ_α results in

$$\frac{\partial J}{\partial \Theta_\alpha^\top} = -\sum_{i=1}^{3n} \Phi(\alpha_i) \left[y_i - \Phi^\top(\alpha_i)\Theta_\alpha \right] \tag{7}$$

The minimum error squared is obtained by setting $\frac{\partial J}{\partial \Theta_\alpha^\top}$ equal to zero, thereby resulting in

$$\sum_{i=1}^{3n} \Phi(\alpha_i)\Phi^\top(\alpha_i)\Theta_\alpha = \sum_{i=1}^{3n} \Phi(\alpha_i) y_i \tag{8}$$

Let $H_{n-1} = \sum_{i=1}^{3n} \Phi(\alpha_i)\Phi^\top(\alpha_i)$ and $V_{n-1} = \sum_{i=1}^{3n} \Phi(\alpha_i) y_i$ where $n = 1, 2, \ldots, N$. Then,

$$\Theta_\alpha^{(n-1)} = H_{n-1}^{-1} V_{n-1} \tag{9}$$

where

$$H_{n-1} = \begin{bmatrix} \sum_{i=1}^{3n} \alpha_i^4 & \sum_{i=1}^{3n} \alpha_i^3 & \sum_{i=1}^{3n} \alpha_i^2 \\ \sum_{i=1}^{3n} \alpha_i^3 & \sum_{i=1}^{3n} \alpha_i^2 & \sum_{i=1}^{3n} \alpha_i \\ \sum_{i=1}^{3n} \alpha_i^2 & \sum_{i=1}^{3n} \alpha_i & \sum_{i=1}^{3n} 1 \end{bmatrix} \tag{10}$$

$$V_{n-1} = \begin{bmatrix} \sum_{i=1}^{3n} \alpha_i^2 \Delta C_{L_i} & \sum_{i=1}^{3n} \alpha_i^2 \Delta C_{D_i} & \sum_{i=1}^{3n} \alpha_i^2 \Delta C_{m_i} \\ \sum_{i=1}^{3n} \alpha_i \Delta C_{L_i} & \sum_{i=1}^{3n} \alpha_i \Delta C_{D_i} & \sum_{i=1}^{3n} \alpha_i \Delta C_{m_i} \\ \sum_{i=1}^{3n} \Delta C_{L_i} & \sum_{i=1}^{3n} \Delta C_{D_i} & \sum_{i=1}^{3n} \Delta C_{m_i} \end{bmatrix} \tag{11}$$

During the first iteration, $n = 3$ as there are three data points. During subsequent iterations, three more data points per iteration are added. A RLS algorithm is developed to enable the current parameter estimation to take advantage of the previous parameter estimates. The regression equation for the next iteration is formed as

$$\Theta_\alpha^{(n)} = H_n^{-1} V_n \tag{12}$$

But H_n and V_n can be written as

$$H_n = \sum_{i=1}^{3n} \Phi(\alpha_i)\Phi^\top(\alpha_i) + \sum_{i=1}^{3} \Phi(\alpha_i)\Phi^\top(\alpha_i) = H_{n-1} + H_0 \tag{13}$$

$$V_n = \sum_{i=1}^{3n} \Phi(\alpha_i) y_i + \sum_{i=1}^{3} \Phi(\alpha_i) y_i = H_{n-1}\Theta_\alpha^{(n-1)} + V_0 \tag{14}$$

where $H_0 = \sum_{i=1}^{3} \Phi(\alpha_i)\Phi^\top(\alpha_i)$ and $V_0 = \sum_{i=1}^{3} \Phi(\alpha_i) y_i^\top$ are evaluated using the past data. Therefore, the RLS algorithm can be written as

$$\Theta_\alpha^{(n)} = (H_{n-1} + H_0)^{-1} \left(H_{n-1}\Theta_\alpha^{(n-1)} + V_0 \right) \tag{15}$$

The sensitivities of the aerodynamic coefficients with respect to the flap deflections are estimated in the second stage. During this stage, the mini-plain flaps and the elevator are perturbed one at a time by $\pm\Delta\delta$ where $\Delta\delta$ is a chosen increment. The angle of attack is kept constant during this perturbation. A linear regression can be performed by minimizing the error squared

$$\min J = \sum_{i=1}^{2n} \left(\begin{bmatrix} \delta C_L \\ \delta C_D \\ \delta C_m \end{bmatrix}_i - \begin{bmatrix} C_{L_\delta} \\ C_{D_\delta} \\ C_{m_\delta} \end{bmatrix} \delta_i - \begin{bmatrix} C_{L_{\delta^2}} \\ C_{D_{\delta^2}} \\ C_{m_{\delta^2}} \end{bmatrix} \delta_i^2 \right)^2 \tag{16}$$

where $\delta = \begin{bmatrix} \delta_1 & \delta_2 & \cdots & \delta_{11} & \delta_e \end{bmatrix}^\top$ is redefined to include the elevator deflection and

$$\begin{bmatrix} \delta C_L \\ \delta C_D \\ \delta C_m \end{bmatrix} = \begin{bmatrix} C_L \\ C_D \\ C_m \end{bmatrix} - \begin{bmatrix} \bar{C}_L \\ \bar{C}_D \\ \bar{C}_m \end{bmatrix} \tag{17}$$

where

$$\begin{bmatrix} \bar{C}_L \\ \bar{C}_D \\ \bar{C}_m \end{bmatrix} = \begin{bmatrix} C_{L_0} \\ C_{D_0} \\ C_{m_0} \end{bmatrix} + \begin{bmatrix} C_{L_\alpha} \\ C_{D_\alpha} \\ C_{m_\alpha} \end{bmatrix} \bar{\alpha} + \begin{bmatrix} C_{L_{\alpha^2}} \\ C_{D_{\alpha^2}} \\ C_{m_{\alpha^2}} \end{bmatrix} \bar{\alpha}^2 - \begin{bmatrix} C_{L_\delta} \\ C_{D_\delta} \\ C_{m_\delta} \end{bmatrix} \bar{\delta} - \begin{bmatrix} C_{L_{\delta^2}} \\ C_{D_{\delta^2}} \\ C_{m_{\delta^2}} \end{bmatrix} \bar{\delta}^2 \tag{18}$$

But the flap deflection vector δ for the perturbed flap k is expressed as

$$\delta_j = \begin{cases} \bar{\delta}_j & j \neq k \\ \bar{\delta}_j + \Delta\delta_k & j = k \end{cases} \tag{19}$$

where $\Delta\delta_k = \pm\Delta\delta$ during the perturbation cycle. Therefore, we see that

$$\begin{bmatrix} \delta C_L \\ \delta C_D \\ \delta C_m \end{bmatrix} = \begin{bmatrix} C_{L_\delta} \\ C_{D_\delta} \\ C_{m_\delta} \end{bmatrix} \Delta\delta_k + \begin{bmatrix} C_{L_{\delta^2}} \\ C_{D_{\delta^2}} \\ C_{m_{\delta^2}} \end{bmatrix} \Delta\delta_k^2 + \begin{bmatrix} C_{L_{\delta_e}} \\ C_{D_{\delta_e}} \\ C_{m_{\delta_e}} \end{bmatrix} \Delta\delta_e + \begin{bmatrix} C_{L_{\delta_e^2}} \\ C_{D_{\delta_e^2}} \\ C_{m_{\delta_e^2}} \end{bmatrix} \Delta\delta_e^2 \tag{20}$$

where $\Delta\delta_e = \pm\Delta\delta$.

We denote $z_i = \begin{bmatrix} \delta C_L \\ \delta C_D \\ \delta C_m \end{bmatrix}_i$, $\Theta_{\delta_k} = \begin{bmatrix} C_{L_{\delta_k^2}} & C_{D_{\delta_k^2}} & C_{m_{\delta_k^2}} \\ C_{L_{\delta_k}} & C_{D_{\delta_k}} & C_{m_{\delta_k}} \end{bmatrix}$, $k = 1, 2\cdots, 12$, and $\Phi(\Delta\delta_i) = \begin{bmatrix} \Delta\delta_{k,i}^2 \\ \Delta\delta_{k,i} \end{bmatrix}$. Then, the cost function to minimize the error squared is

$$\min J = \sum_{i=1}^{2n} \left[z_i - \Theta_\delta^\top \Phi(\Delta\delta_i) \right]^2 \tag{21}$$

The parameter estimates of the sensitivities of the aerodynamic coefficients with respect to the flap deflections are computed as

$$\Theta_{\delta_k}^{(n-1)} = G_{n-1}^{-1} U_{n-1} \tag{22}$$

where

$$G_{n-1} = \sum_{i=1}^{2n} \Phi(\Delta\delta_i) \Phi^\top(\Delta\delta_i) = \begin{bmatrix} \sum_{i=1}^{2n} \Delta\delta_{k,i}^4 & \sum_{i=1}^{2n} \Delta\delta_{k,i}^3 \\ \sum_{i=1}^{2n} \Delta\delta_{k,i}^3 & \sum_{i=1}^{2n} \Delta\delta_{k,i}^2 \end{bmatrix} \tag{23}$$

$$U_{n-1} = \sum_{i=1}^{2n} \Phi(\Delta\delta_i) z_i^\top = \begin{bmatrix} \sum_{i=1}^{2n} \Delta\delta_{k,i}^2 \delta C_{L_i} & \sum_{i=1}^{2n} \Delta\delta_{k,i}^2 \delta C_{D_i} & \sum_{i=1}^{2n} \Delta\delta_{k,i}^2 \delta C_{m_i} \\ \sum_{i=1}^{2n} \Delta\delta_{k,i}^2 \delta C_{L_i} & \sum_{i=1}^{2n} \Delta\delta_{k,i} \delta C_{D_i} & \sum_{i=1}^{2n} \Delta\delta_{k,i} \delta C_{m_i} \end{bmatrix} \tag{24}$$

The RLS algorithm is also established as

$$\Theta_{\delta_k}^{(n)} = (G_{n-1} + G_0)^{-1} \left(G_{n-1} \Theta_{\delta_k}^{(n-1)} + U_0 \right) \tag{25}$$

where $G_0 = \sum_{i=1}^{2} \Phi(\Delta\delta_i) \Phi^\top(\Delta\delta_i)$ and $U_0 = \sum_{i=1}^{2} \Phi(\Delta\delta_i) z_i^\top$ are computed from the past data.

IV. Drag Optimization

To minimize drag, we consider the following cost function:

$$\min J = C_D + \lambda_L \left(\bar{C}_L - C_L \right) + \lambda_m \left(\bar{C}_m - C_m \right) \tag{26}$$

where λ_L and λ_m are the adjoint variables for the lift and pitching moment.

Evaluating the partial derivatives of the cost function yields

$$\frac{\partial J}{\partial \alpha} = C_{D_\alpha} + 2C_{D_{\alpha^2}} \alpha - \lambda_L \left(C_{L_\alpha} + 2C_{L_{\alpha^2}} \alpha \right) - \lambda_m \left(C_{m_\alpha} + 2C_{m_{\alpha^2}} \alpha \right) \tag{27}$$

$$\frac{\partial J}{\partial \delta^\top} = C_{D_\delta}^\top + 2\text{diag}\left(C_{D_{\delta^2}} \right) \delta - \lambda_L \left[C_{L_\delta}^\top + 2\text{diag}\left(C_{L_{\delta^2}} \right) \delta \right] - \lambda_m \left[C_{m_\delta}^\top + 2\text{diag}\left(C_{m_{\delta^2}} \right) \delta \right] \tag{28}$$

$$\frac{\partial J}{\partial \delta_e} = C_{D_{\delta_e}} + 2C_{D_{\delta_e^2}} \delta_e - \lambda_L \left(C_{L_{\delta_e}} + 2C_{L_{\delta_e^2}} \delta_e \right) - \lambda_m \left(C_{m_{\delta_e}} + 2C_{m_{\delta_e^2}} \delta_e \right) \tag{29}$$

$$\frac{\partial J}{\partial \lambda_L} = \bar{C}_L - C_L \tag{30}$$

$$\frac{\partial J}{\partial \lambda_m} = \bar{C}_m - C_m \tag{31}$$

where $\bar{C}_m = 0$ at trim. Setting $\frac{\partial J}{\partial \alpha}$ and $\frac{\partial J}{\partial \delta_e}$ to zero yields

$$\begin{bmatrix} \lambda_L \\ \lambda_m \end{bmatrix} = \begin{bmatrix} C_{L_\alpha} + 2C_{L_{\alpha^2}}\alpha & C_{m_\alpha} + 2C_{m_{\alpha^2}}\alpha \\ C_{L_{\delta_e}} + 2C_{L_{\delta_e^2}}\delta_e & C_{m_{\delta_e}} + 2C_{m_{\delta_e^2}}\delta_e \end{bmatrix}^{-1} \begin{bmatrix} C_{D_\alpha} + 2C_{D_{\alpha^2}}\alpha \\ C_{D_{\delta_e}} + 2C_{D_{\delta_e^2}}\delta_e \end{bmatrix} \tag{32}$$

Note that each the current iteration, λ_L and λ_m are computed from the previous values of α and δ_e. The optimal flap deflections are then obtained by setting $\frac{\partial J}{\partial \delta^\top} = 0$ which results in

$$\delta = \frac{1}{2}\left[\text{diag}\left(C_{D_{\delta^2}} - \lambda_L C_{L_{\delta^2}} - \lambda_m C_{m_{\delta^2}}\right)\right]^{-1}\left(-C_{D_\delta}^\top + \lambda_L C_{L_\delta}^\top + \lambda_m C_{m_\delta}^\top\right) \tag{33}$$

The flap deflections are subject to the position limits which require $\delta_{min} \leq \delta \leq \delta_{max}$ where δ_{min} and δ_{max} are the minimum and maximum flap deflection vectors.

Setting $\frac{\partial J}{\partial \lambda_L} = 0$ and $\frac{\partial J}{\partial \lambda_m} = 0$ yields the lift and pitching moment coefficient constraint equations

$$\bar{C}_L = C_{L_0} + C_{L_\alpha}\alpha + C_{L_\delta}\delta + C_{L_{\delta_e}}\delta_e + C_{L_{\alpha^2}}\alpha^2 + C_{L_{\delta^2}}\delta^2 + C_{L_{\delta_e^2}}\delta_e^2 \tag{34}$$

$$0 = C_{m_0} + C_{m_\alpha}\alpha + C_{m_\delta}\delta + C_{m_{\delta_e}}\delta_e + C_{m_{\alpha^2}}\alpha^2 + C_{m_{\delta^2}}\delta^2 + C_{m_{\delta_e^2}}\delta_e^2 \tag{35}$$

from which α and δ_e can be updated using the current values of δ computed from Eq. (33). Equations (34) and (35) are nonlinear but can be solved using the nonlinear root search.

V. Simulation Results

Simulations of the real-time drag optimization are conducted. All the sensitivities are initially set to zero. The target lift coefficient is 0.5. At each optimization iteration, the perturbations of the angle of attack and the flap deflections are carried out to estimate the sensitivities. Using the newly computed sensitivities, the drag optimization is computed to obtain the trim angle of attack, the trim flap deflections, and the trim elevator deflections. The iterations continue until the lift coefficient converges within a certain tolerance. Table 1 shows the results of the real-time drag optimization for Mach 0.80, Mach 0.85, and Mach 0.88. The largest drag reduction is 3.37% corresponding to Mach 0.85. This is consistent with the fact that the maximum L/D for Mach 0.85 occurs at a lift coefficient that is furthest away from the design lift coefficient of 0.5. A drag reduction of 2.46% is obtained for Mach 0.80 and 1.95% for Mach 0.88.

	C_D	C_D Reduction	α	δ_e
Baseline @ Mach 0.8	0.01857	0%	2.51°	2.45°
Drag Optimization @ Mach 0.8	0.01812	2.46%	2.69°	-0.49°
Baseline @ Mach 0.85	0.02152	0%	2.30°	2.52°
Drag Optimization @ Mach 0.85	0.02080	3.37%	2.53°	0.37°
Baseline @ Mach 0.88	0.02455	0%	2.25°	2.50°
Drag Optimization @ Mach 0.88	0.02407	1.95%	2.06°	0.80°

Table 1. Real-Time Drag Optimization Results for AR 13.5 CRM

Figure 16 shows the deflections of the mini-plain flaps for Mach 0.80, Mach 0.85, and Mach 0.88. Note that the mini-plain flaps 4, 5, 10, and 11 are saturated at the maximum limit of 10° for Mach 0.88. The trend from the drag optimization indicates that the lift distribution needs to be reduced at the inboard and needs to be increased at the outboard toward the tip.

Figures 17, 18, and 19 show the convergence of the lift, drag, and pitching moment coefficients, respectively, during the real-time drag optimization of the Mach 0.85 configuration. The drag coefficient converges rapidly after 5 iterations. The lift and pitching moment coefficients on the other hand start to converge after 12 iterations.

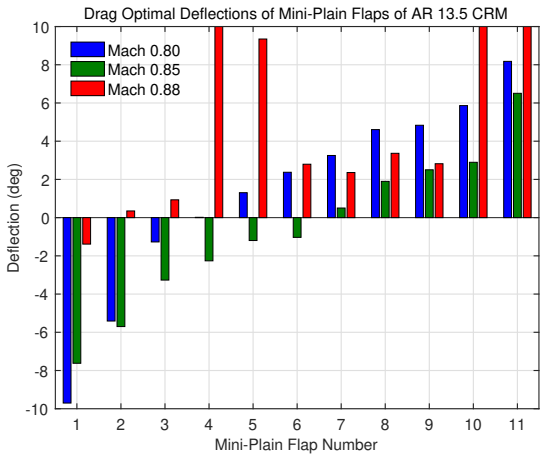

Figure 16. Deflections of Mini-Plain Flaps for Real-Time Drag Optimization of AR 13.5 CRM for Mach 0.85

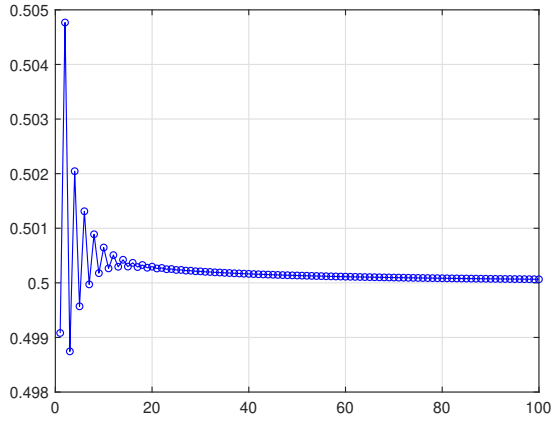

Figure 17. Lift Coefficient C_L Convergence of Real-Time Drag Optimization of AR 13.5 CRM for Mach 0.85

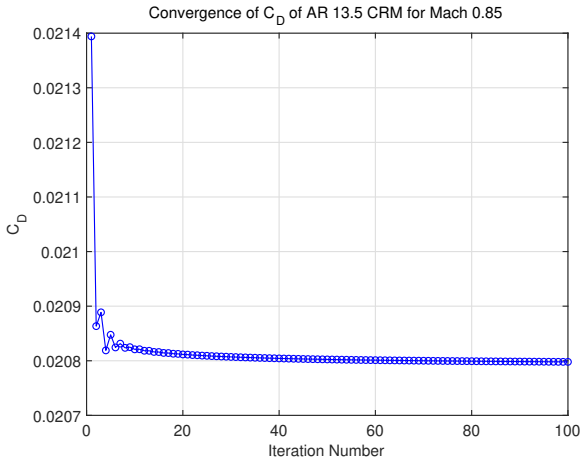

Figure 18. Drag Coefficient C_D Convergence of Real-Time Drag Optimization of AR 13.5 CRM for Mach 0.85

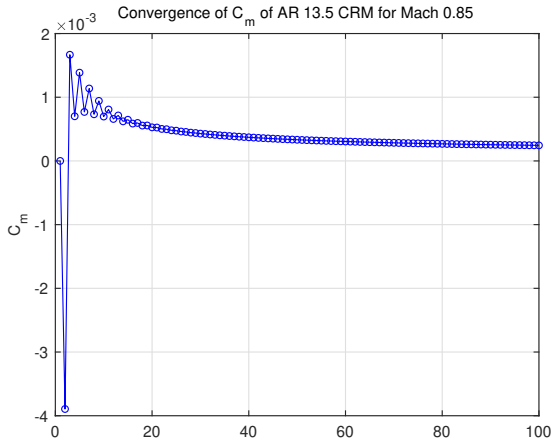

Figure 19. Pitching Moment Coefficient C_m Convergence of Real-Time Drag Optimization of AR 13.5 CRM for Mach 0.85

Figures 20, 21, and 22 show the convergence of the parameter estimation of the sensitivities C_{L_α} and $C_{L_{\alpha^2}}$, C_{D_α} and $C_{D_{\alpha^2}}$, and C_{m_δ} and $C_{m_{\delta^2}}$ with respect to the angle of attack, respectively. The sensitivities $C_{L_{\alpha^2}}$, $C_{D_{\alpha^2}}$, and $C_{m_{\delta^2}}$ are slower to converge than the sensitivities C_{L_α}, C_{D_α}, and C_{m_δ}.

Figures 23 and 24 show the convergence of the parameter estimation of the sensitivities C_{L_δ} and $C_{L_{\delta^2}}$ with respect to the deflections of the mini-plain flaps, respectively.

Figures 25 and 26 show the convergence of the parameter estimation of the sensitivities C_{D_δ} and $C_{D_{\delta^2}}$ with respect to the deflections of the mini-plain flaps, respectively.

Figures 27 and 28 show the convergence of the sensitivities C_{m_δ} and $C_{m_{\delta^2}}$ with respect to the deflections of the mini-plain flaps, respectively.

Figure 29 shows the convergence of the parameter estimation of the sensitivities $C_{L_{\delta_e}}$, $C_{L_{\delta_e^2}}$, $C_{D_{\delta_e}}$, $C_{D_{\delta_e^2}}$, $C_{m_{\delta_e}}$, and $C_{m_{\delta_e^2}}$ with respect to the elevator deflection.

The parameter convergence of the sensitivities with respect to the deflections of the mini-plain flaps and the elevator is observed to be excellent with most parameter estimates reaching their constant values after about 10 iterations.

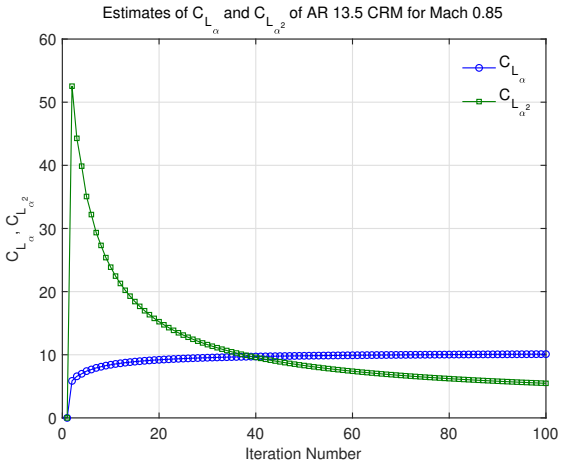

Figure 20. Estimates of C_{L_α} and $C_{L_{\alpha^2}}$ Sensitivities of AR 13.5 CRM for Mach 0.85

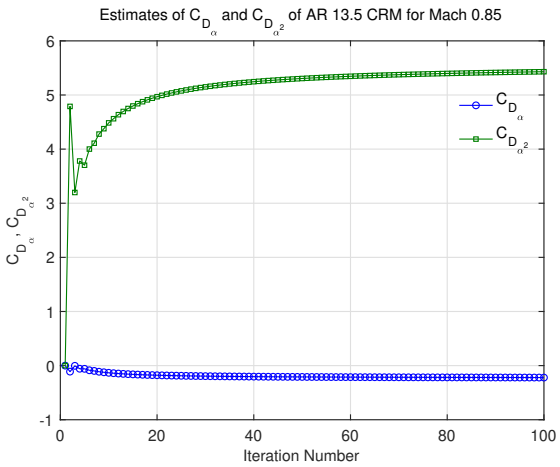

Figure 21. Estimates of $C_{D\alpha}$ and $C_{D_{\alpha^2}}$ Sensitivities of AR 13.5 CRM for Mach 0.85

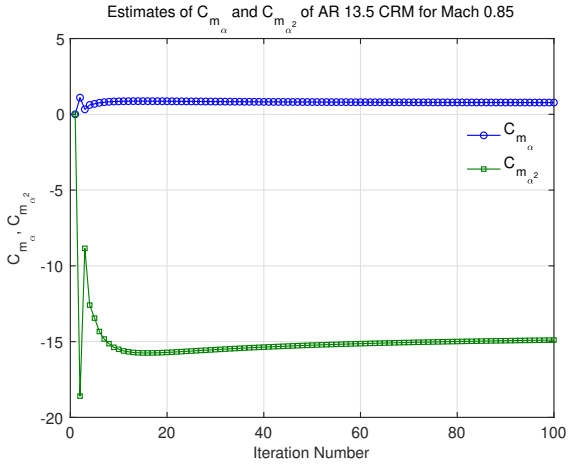

Figure 22. Estimates of $C_{m\alpha}$ and $C_{m_{\alpha^2}}$ Sensitivities of AR 13.5 CRM for Mach 0.85

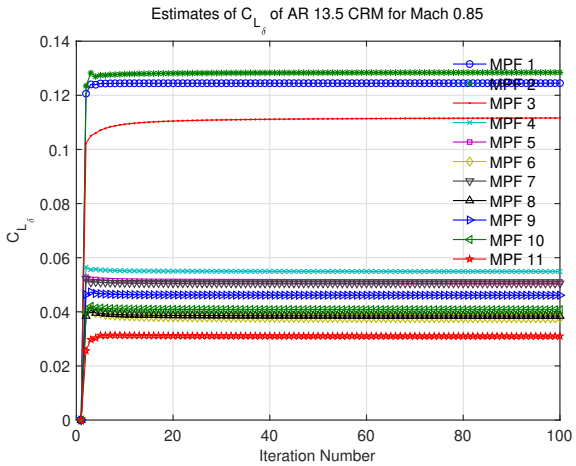

Figure 23. Estimates of C_{L_δ} Sensitivities of AR 13.5 CRM for Mach 0.85

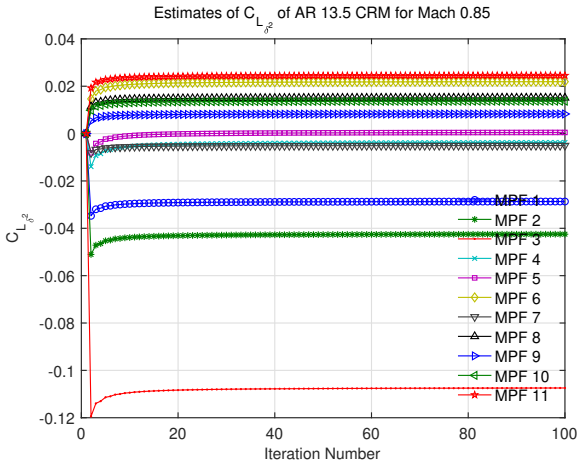

Figure 24. Estimates of $C_{L_{\delta^2}}$ Sensitivities of AR 13.5 CRM for Mach 0.85

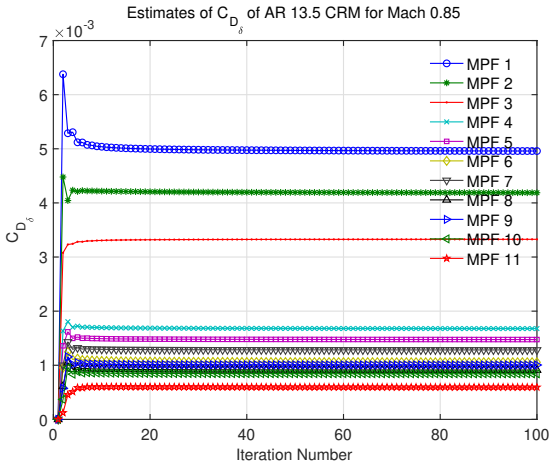

Figure 25. Estimates of C_{D_δ} Sensitivities of AR 13.5 CRM for Mach 0.85

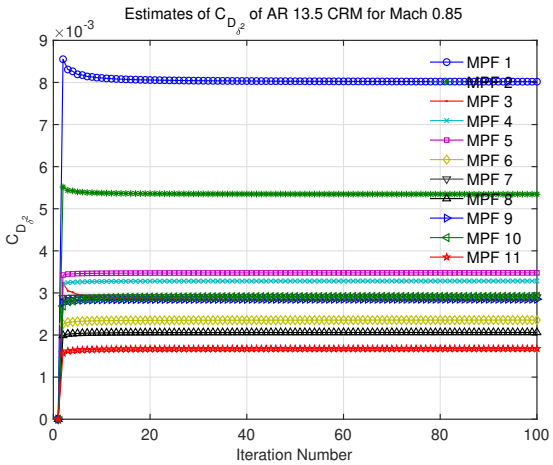

Figure 26. Estimates of $C_{D_{\delta^2}}$ Sensitivities of AR 13.5 CRM for Mach 0.85

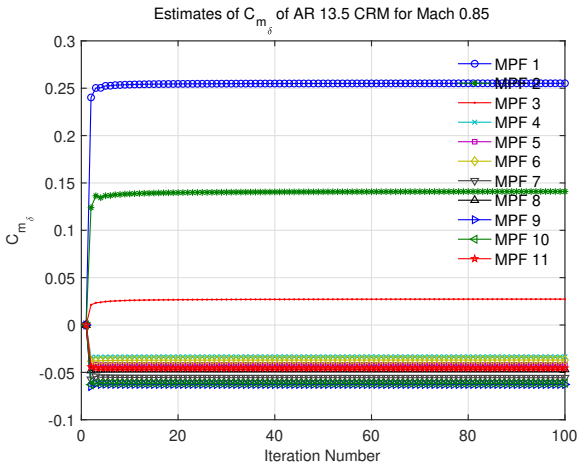

Figure 27. Estimates of C_{m_δ} Sensitivities of AR 13.5 CRM for Mach 0.85

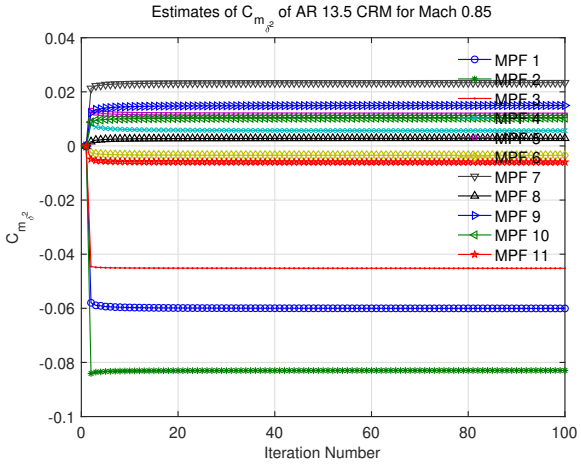

Figure 28. Estimates of $C_{m_{\delta^2}}$ Sensitivities of AR 13.5 CRM for Mach 0.85

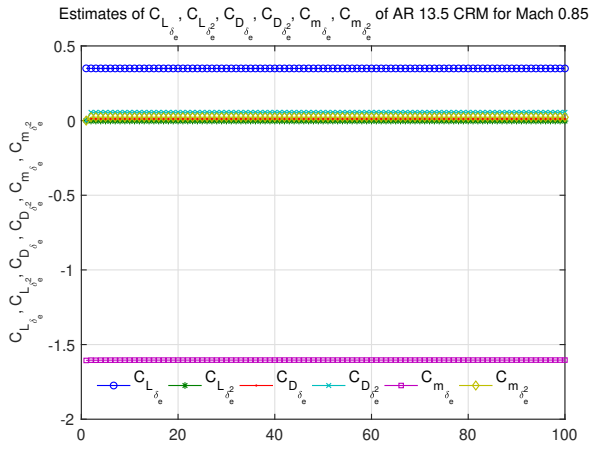

Figure 29. Estimates of $C_{L_{\delta_e}}$, $C_{L_{\delta_e^2}}$, $C_{D_{\delta_e}}$, $C_{D_{\delta_e^2}}$, $C_{m_{\delta_e}}$, $C_{m_{\delta_e^2}}$ Sensitivities of AR 13.5 CRM for Mach 0.85

VI. Conclusions

This paper presents a real-time drag optimization study for the aspect ratio 13.5 Common Research Model developed by Boeing. The aircraft configuration is equipped with 11 mini-plain flaps. An aerodynamic database computed by Boeing TRANAIR code is used in the study. An onboard aerodynamic model is constructed to model the lift, drag, and pitching moment coefficients as functions of the angle of attack, the mini-plain flap deflections, and the elevator deflection. A recursive least-squares parameter estimation is developed to estimate the sensitivities of the aerodynamic model with respect to the angle of attack, the flap deflections, and the elevator deflection. The parameter estimation is a two-stage process. During the first stage, only the sensitivities with respect to the angle of attack are estimated by applying excitation signals to the angle of attack while maintaining the flap deflections constant. During the second stage, the sensitivities with respect to the flap deflections and the elevator deflection are estimated by applying excitation signals to the mini-plain flaps and the elevator. Simulations are conducted for Mach 0.80, Mach 0.85, and Mach 0.88. The results of the real-time drag optimization show a drag reduction of 2.46%, 3.37%, and 1.95% for Mach 0.80, Mach 0.85, and Mach 0.88, respectively. The parameter estimation achieves an excellent parameter convergence.

Acknowledgment

The authors wish to acknowledge NASA Advanced Air Transport Technology (AATT) project for the funding support of this work. The authors also wish to acknowledge Boeing Research and Technology, in particular Dr. John Quindlen, for providing the aerodynamic data to support this work under NASA contract NNL15AA00A with the AATT project.

References

[1]Ferrier, Y., Nguyen, N., and Ting, E., "Real-Time Adaptive Least-Squares Drag Minimization for Performance Adaptive Aeroelastic Wing," 34th AIAA Applied Aerodynamics Conference, AIAA-2016-3567, June 2016.

[2]Precup, N., Mundt, T., Mor, M., Livne, E., "An Active Variable Camber Continuous Trailing Edge Flapped Wing Wind Tunnel Model for Aeroelastic "In-Flight" Shape Optimization Tests," AIAA Multidisciplinary Analysis and Optimization Conference, AIAA-2018-3106, June 2018.

[3]Nguyen, N., Cramer, N., Hashemi, K., Drew, M., Wise, R., Boskovic, J., Mundt, T., Precup, N., and Livne, E., "Real-Time Adaptive Drag Minimization Wind Tunnel Investigation of a Flexible Wing with Variable Camber Continuous Trailing Edge Flap System," AIAA Applied Aerodynamic Conference, AIAA-2019-3156, June 2019.

[4]Vassberg, J., Dehaan M., Rivers, M., and Wahls, R., "Development of a Common Research Model for Applied CFD Validation Studies," 26th AIAA Applied Aerodynamics Conference, AIAA-2008-6919, August 2008.